Geomechanics and Engineering, *Vol. 34, No. 1 (2023) 1-15*
https://doi.org/10.12989/gae.2023.34.1.001

Time-frequency domain characteristics of intact and cracked red sandstone based on acoustic emission waveforms

Yong Niu[1,2,3a], Jinguo Wang[3b], Yunjin Hu[*1,2], Gang Wang[1,2c] and Bolong Liu[1,2d]

[1]*Key Laboratory of Rock Mechanics and Geohazards of Zhejiang Province, Shaoxing University, Shaoxing 312099, Zhejiang China*
[2]*School of Civil Engineering, Shaoxing University, Shaoxing 312099, Zhejiang China*
[3]*School of Earth Science and Engineering, Hohai University, Nanjing 211100, Jiangsu China*

(*Received May 19, 2022, Revised April 11, 2023, Accepted April 18, 2023*)

Abstract. This study conducts uniaxial compression tests on intact and single crack-contained rocks to investigate the time-frequency domain characteristics of acoustic emission (AE) signals monitored during the deformation failure process. A processing approach, short-time Fourier transform (STFT), is performed to obtain the evolution characteristics of time-frequency domain of AE signals. The AE signal modes at different deformation stages of rocks are different. Five modes of AE signal are observed during the cracking process of rocks. The evolution characteristics of time-frequency domain of AE signals processed by STFT can be utilized to evaluate the damage process of rocks. The difference of time-frequency domain characteristics between intact and cracked rocks is comparatively analyzed. The distribution characteristics of frequency changing from a single band-shaped cluster to multiple band-shaped clusters can be regarded as an early warning information of damage and failure of rocks. Meanwhile, the attenuation of frequency enables the exploration of rock failure trends.

Keywords: acoustic emission (AE); cracked rock; damage; early warning; time-frequency analysis

1. Introduction

Part of energy stored within rocks under high compression stress is rapidly released in the form of elastic perturbation wave, which is called the phenomenon of Acoustic emission (AE) (Liu *et al.* 2015, Moradian *et al.* 2016, Niu and Zhou 2021, Huang *et al.* 2022). The wave amplitude and frequency components for AE signals generated from rocks contain some important information related to the failure mechanism of rocks (Zhang *et al.* 2016). Consequently, investigating these AE signals contributes to deduce the changes in mechanical properties of rocks and to further to invert failure mechanism of rocks. At present, AE technology has been proved to be a nondestructive and effective monitoring tool, which can be used to evaluate the damage evolution process of rock materials (Shukla *et al.* 2013, Liu *et al.* 2015, Moradian *et al.* 2016, Niu *et al.* 2019, Zhou and Zhang 2021).

Rocks are a complex heterogeneous geological material containing many pre-existing cracks (Wong and Einstein 2009, Berto and Lazzarin 2014, Yang *et al.* 2014, Lin *et al.* 2015, Zhu and Liu 2018, Pakzad *et al.* 2018, Zhou *et al.* 2019, Shi *et al.* 2020, Kong *et al.* 2021, Liu *et al.* 2021, Zhao *et al*. 2022, Niu *et al*. 2023a). These pre-existing cracks result in the complex cracking process of rocks (Zhao *et al.* 2015, Wang *et al.* 2017, Wang *et al.* 2018, Sun *et al.* 2019, Niu and Zhou 2021, Liu *et al.* 2021). However, how to effectively characterize this complex cracking process of rocks containing pre-existing cracks is a difficult problem for reliably assessing the stability and safety in underground rock engineering at present (Berto *et al.* 2013, Zhang *et al.* 2018). Luckily, AE monitoring technology provides an effective way to characterize the fracture damage process of rocks containing pre-existing cracks.

The processing methods about AE signals can roughly be classified into three categories based on previous studies (Zhang *et al.* 2015, Li *et al.* 2017, Niu and Zhou 2021), including parameter-based analysis method, source localization-based analysis method and waveform-based analysis method. For the method of AE parameter analysis, the evolution characteristics of some conventional time series parameters (counts, energy, amplitude, etc.) are widely used to investigate the damage evolution process of rocks, which is due to the convenience of obtaining these parameters (Wasantha *et al.* 2014, Miao *et al.* 2021, Zheng *et al.* 2021). For example, Wasantha *et al.* (2014) conducted uniaxial compression tests on bedded-sandstone using AE monitoring technology and constructed the relationship between the AE energy and the damage process of rocks. Miao *et al.* (2021) adopted the AE count rate to investigate the deformation failure process of granite exposed to different temperatures under uniaxial compression. Zheng *et al.* (2021) used two AE parameters, including AE energy and cumulative count, to characterize the cracking process of sandstone subjected to uniaxial compression. These studies are vital to understand the failure mechanism of rocks. However, AE parameter analysis method presents the

∗Corresponding author, Ph.D. Candidate
E-mail: YunjinHusxu@126.com
[a]Ph.D.
[b]Professor
[c]Ph.D.
[d]Ph.D.

ISSN: 2005-307X (Print), 2092-6219 (Online)

limited information of AE source (Zhang *et al.* 2016). The damage failure of rocks is a multi-scalar and nonlinear dynamic process (He *et al.* 2010). Therefore, the evolution characteristics of conventional AE parameters have distinct uncertainty due to the nonstationary and stochastic properties of AE signals.

AE localization technique can visualize the fracture paths within rocks, which primarily uses a multichannel signal acquisition system to obtain the time arrived from cracking event source to different AE probes. This method has been employed to trace the fracture evolution process of rocks subjected to compression stress (Zhang *et al.* 2015, Wong and Xiong 2018). Zhang *et al.* (2015) carried out uniaxial and triaxial compression tests on granite to study the spatial cracking evolution characteristics of rocks via AE localization technology. Wong and Xiong (2018) used AE localization technique to analyze the cracking process of marble specimen containing a single pre-existing crack under uniaxial compression. These studies suggest that the failure mechanism of rocks under compression can be well analyzed. Nevertheless, the numbers of AE probes directly determine the accuracy of AE event localization, leading to that this approach has a certain limitation in field application due to the arrangement of AE probes.

AE waveform signals contain lots of information of AE source, which promotes that AE waveform analysis method becomes a new studying hotspot lately. At present, some scholars focus mainly on dynamic frequency spectrum characteristics of AE waveform during the loading process of rocks (He *et al.* 2010, Lu *et al.* 2012, Li *et al.* 2017, Zheng *et al.* 2018, Wang *et al.* 2019). For example, He *et al.* (2010) utilized the evolution characteristics of dominant frequency for AE waveform to investigate the rock burst process of limestone under true-triaxial unloading conditions. Zheng *et al.* (2018) performed uniaxial compression tests on marble to quantitatively investigate the failure mechanisms of rocks based on the evolution characteristics of dominant frequency of AE signals. These researches enhance the understanding in spectrum characteristics of AE signals related to the rock damage. However, previous studies primarily concentrate on time-varying evolution characteristics of dominant frequency of AE waveforms, resulting in that the complexity and globality of time-frequency domain characteristics of AE signals are neglected. The time-frequency domain analysis of AE signals can present the spectral components in the different times (Benson *et al.* 2010, Zhang *et al.* 2016, Li *et al*. 2021). Consequently, in this study, time-frequency domain analysis of AE waveforms will be studied to understand the failure mechanism of rocks and to explore the precursor characteristics of instability.

With that in mind, this paper conducts uniaxial compression tests on intact and cracked red sandstone specimens. Both AE monitoring and photographic capturing techniques are employed to record the cracking process of rocks in real time. The objective of this study is to present the time-frequency domain analysis of AE signals monitored during cracking process of rocks under uniaxial compression. The damage mechanism of rocks is studied by the evolution characteristics of time-frequency domain of AE signals. The difference between the time-frequency domain characteristics of intact and cracked rocks is analyzed. Moreover, the precursor information of rocks instability is studied and discussed based on the evolution characteristics of time-frequency domain of AE signals.

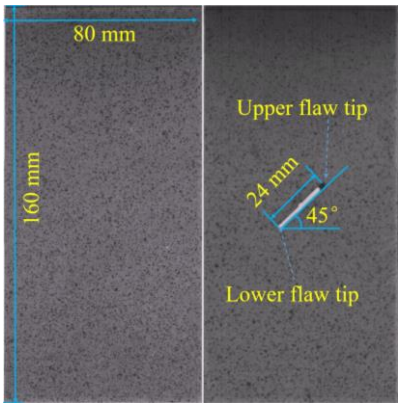

Fig. 1 Geometry of tested specimens

2. Experimental materials and methods

2.1 Experimental materials

The rock materials used in this study were selected as red sandstone and gathered from Chongqing city of China. The rock materials were machined as the rectangular prismatic specimens with dimensions of 160×80×30 mm. The specimens were cut from the same rock block along the same direction to reduce the effects of rock anisotropy on experimental results. To ensure a uniform stress state within specimens, the height-to-width ratio of specimens was fixed to 2.0. The geometries of intact specimen and specimen containing pre-existing crack are shown in Fig. 1. A single crack with the width of 1 mm in specimen was prefabricated using a high-pressure water jet. In Fig. 1, the length of crack is 24 mm, the inclination angle of crack (i.e., the angle of crack with the horizontal direction) is 45°. The depth of prefabricated crack is the same as the thickness of specimen.

2.2 Experimental methods

In this study, three test systems, including uniaxial compression system, AE monitoring system and high-speed camera capturing system, were simultaneously implemented, as shown in Fig. 2.

Uniaxial compression tests were performed using an AG-250KN IS mechanical servo-controlled testing system. The specimens were compressed at a displacement loading rate of 0.05 mm/min until the ultimate failure occurs. The loading rate of 0.05 mm min^{-1} corresponds to the strain rate of about 5.21×10^{-6} s^{-1}, belonging to the quasi-static loading state. The data, including force, displacement and loading time, were electronically recorded during the loading process of specimens. A VIC-2D high-speed camera was used to record the cracking process of specimens. The

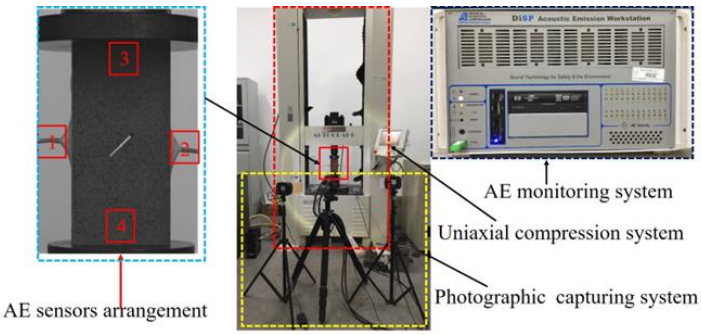

Fig. 2 Experimental test systems used in this study

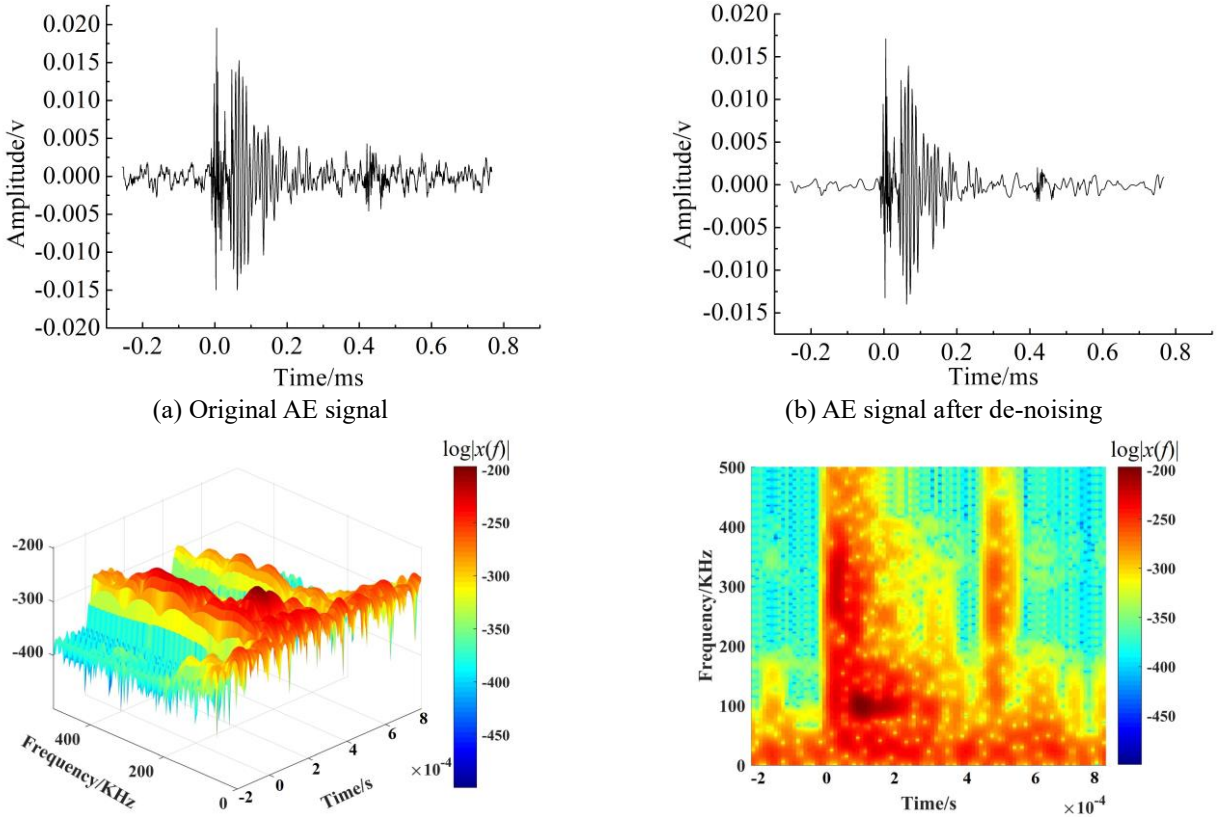

(a) Original AE signal

(b) AE signal after de-noising

(c) Spectrograms in the three-dimensional space

(d) Spectrograms in the two-dimensional space

Fig. 3 Time-frequency domain analysis of AE waveform

details of this recording technique can be found previous study (Zhou *et al*. 2018). The PCI-2 AE monitoring system was employed to record the AE waveforms related to the fracture events of rocks during the loading process. To gain the effective AE signals, the threshold was set to 45 dB, the preamplifier was set to 40 dB, and the sampling rate was set to 1 MHz. The peak definition time, the hit definition time and the hit lockout time were fixed to 300, 800 and 1000 μs, respectively. Besides, the monitoring scale of AE in the laboratory is relatively small, which leads to that the frequency is mainly concentrated in the frequency range of 20 kHz-10 MHz (Li *et al.* 2021). Therefore, NANO-30 AE sensor with a resonant frequency of 300 kHz was selected. Simultaneously, to ensure the accuracies of AE data, four AE sensors were used to monitor the deformation failure process of rocks, as shown in Fig. 2. Vaseline regarded as a couplant was utilized to fill the clearance between the tested specimen and AE sensors. The pencil lead break tests were performed to confirm the validity of AE acquisition system before the specimens are loaded. Note, the AE sensor gathering the most of AE signals during the entire loading process will be selected to analyze the time-frequency domain characteristics of rocks under uniaxial compression. This is mainly due to that the cracking process of rocks usually accompanies with the release of stored energy, which probably leads to that some AE sensors may become loose and AE signals can not be gathered. AE waveform data related to rocks cracking were automatically recorded by the PCI-2 AE monitoring system during the loading process. Each AE waveform was digitally and singly stored in *.csv file.

2.3 AE data processing

In this paper, the short-time Fourier transform (STFT) (Patricia and Celestino 2019) was employed to process the AE waveforms and to obtain the evolution characteristics of time-frequency domain presented as spectrograms. The STFT method can be defined as follows

$$STFT(t, f) = \int_{-\infty}^{\infty} x(t')h(t'-t)\mathrm{e}^{-j2\pi ft'}\mathrm{d}t' \quad (1)$$

Where $x(t)$ is the analysis signal, $h(t'-t)$ is the analysis window functions, t is the sampling time, $STFT(t, f)$ is the frequency spectrum at a given time t.

In addition, the noise processing of AE signals was conducted by the wavelet (Deng *et al.* 2020) before the SFFT processing. The distribution results of time-frequency domain for all of AE waveforms is calculated by MATLAB programming process. Fig. 3 shows the calculation results of a typical AE waveform. Fig. 3(a) is an original AE signal. Fig. 3(b) indicates the AE waveform after de-noising by using wavelet de-noise. Figs. 3(c) and 3(d) show the spectrograms of AE waveform in the three-dimensional and two-dimensional spaces, respectively. In Fig. 3(c), the X-axis shows the time, the Y-axis depicts the frequency, and the Z-axis displays the spectral coefficients |x(f)| shown in a logarithmic dimensionless color scale (log|x(f)|). The intensity of each frequency is represented by the color scale. To convenient visualize the intensity information of each frequency for AE signals, the spectrograms in the two-dimensional space are used to analyze the time-frequency domain characteristics of AE waveform in this study.

3. Mechanical behaviors and fracture process of tested specimens

The cracking evolution process of rocks under uniaxial compression is collectively characterized by AE monitoring and high-speed camera capturing technologies. In this paper, an approach, inter-event time function $F(\tau)$, is performed to present the AE activity monitored during the cracking process of rocks. This approach mainly processes the monitored AE events to obtain the evolution characteristics of AE event rate, which has been proved to be able to characterize the fracture process of rocks. The basic principles of this approach can be found the previous studies (Triantis and Kourkoulis 2018). Moreover, four crack types (Yang *et al.* 2014), i.e., tensile crack (the initiation direction of the crack is perpendicular to the pre-existing crack, and the propagation direction is parallel to the direction of axial stress), tensile crack (the initiation and propagation directions of the crack are parallel to the direction of axial stress) anti-tensile crack (the initiation direction of the crack is opposite that of tensile crack) and far-field crack (the initiation position of the crack is not related to the pre-existing crack), are executed to describe the cracking process of single crack-contained rock specimen, as shown in Fig. 4.

Fig. 5 shows the axial stress-strain curves of intact specimen and cracked specimen under uniaxial

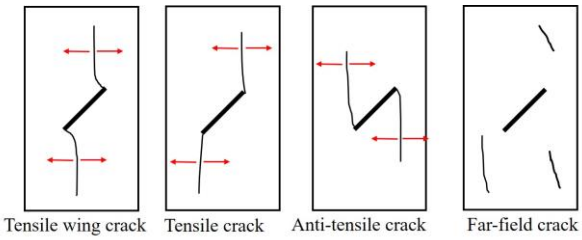

Fig. 4 Four types of cracks describing the cracking behaviors of rock containing pre-existing crack

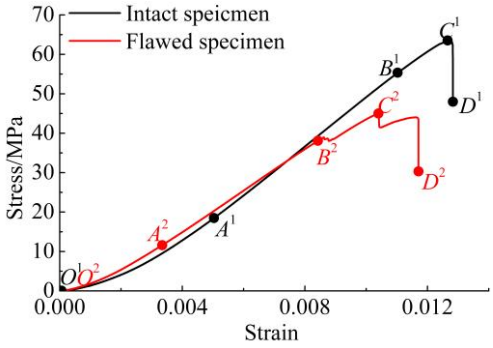

Fig. 5 Axial stress-strain curves for two types of specimens

compression. The deformation process of tested specimens can be divided into four stages based on stress-strain curves. However, the deformation process of intact specimen is different from that of specimen containing pre-existing crack. Namely, the failure process of intact specimen consists of initial nonlinear compaction deformation stage (O^1A^1), linear elastic stage (A^1B^1), yield stage (B^1C^1) and failure stage (C^1D^1). For red sandstone specimen containing pre-existing crack, the deformation process is divided into four stages, including nonlinear compaction deformation stage (O^2A^2), linear elastic stage (A^2B^2), stable macro-cracking stage (B^2C^2) and unstable macro-cracking and failure stage (C^2D^2). Compared to intact specimen, several obvious stress drops occur in the deformation stage of B^2C^2 for red sandstone specimen containing pre-existing crack due to the initiation of new macro-cracks.

Fig. 6 shows the evolution processes of AE event rate and stress versus time for intact specimen subjected to uniaxial compression as well as the ultimate failure modes of specimen. In Fig. 6, no obvious macro-cracking is observed by high-speed camera capturing system before the peak strength of specimen. Simultaneously, the AE event rate is always at the low level. When the specimen is loaded to peak strength, an abrupt increase is observed in AE event rate curve. In the meantime, however, macro-cracking is not observed in the surface of specimen based on the captured images, which is probably due to the occurrence of macro-cracking within specimen. Subsequently, the ultimate failure of intact specimen occurs in a very short time. And a huge failure sonic can be heard and the tested specimen rapidly loses the bearing capacity, which indicates that the red sandstone is a kind of brittle rock material. Whilst AE event rate distinctly increases from low level to high level. Moreover, the ultimate failure modes of intact specimen are mainly dominated by shear fracture, as shown in Fig. 6(b).

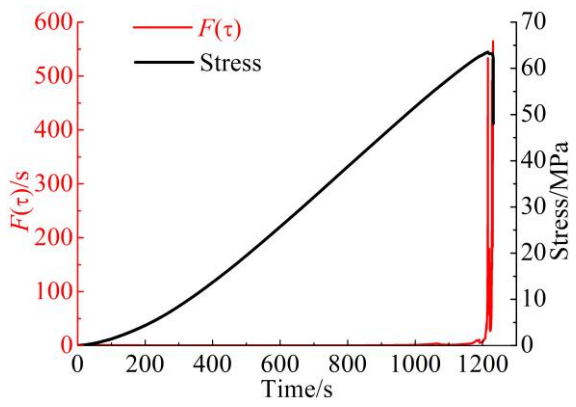

(a) AE event rate and stress versus time

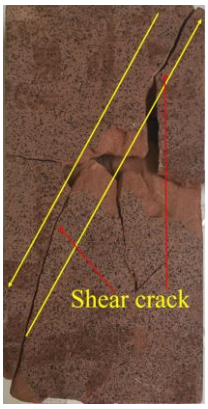

(b) Ultimate failure modes

Fig. 6 Intact red sandstone specimen

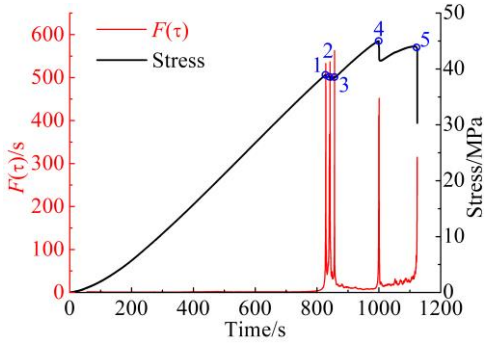

(a) AE event rate and stress versus time

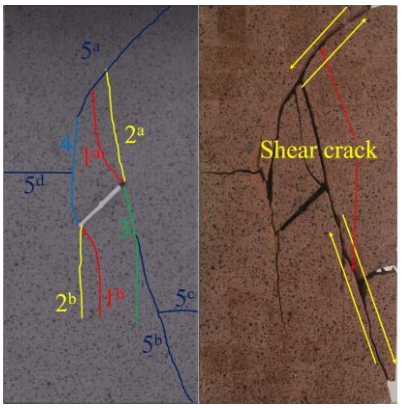

(b) Cracking process and ultimate failure modes

Fig. 7 Red sandstone specimen containing pre-existing crack

Fig. 7 depicts the evolution process of AE event rate and stress versus time for single crack-contained specimen under uniaxial compression as well as the ultimate failure modes of specimen. It can be noted that the numbers in Fig. 7 denote the sequence of macro-cracking observed by photographic capturing system, and the superscript on same numbers indicates that macro-cracks simultaneously initiate from different positions at the same moment. Based on the results of cracking process captured by high-speed camera capturing system, macro-cracking is not observed in the surface of specimen prior to the axial stress of 38.91 MPa. Meanwhile, the AE event rate curve is always at low level. When the axial stress increases to 38.91 MPa (point 1 in Fig. 7(a)), cracks 1^a and 1^b (Tensile wing crack) initiate from the upper and lower tips of crack, and then propagate along the direction of axial stress. In the meantime, AE event rate rapidly increases from low level to high level.

When the specimen is loaded to 38.61 MPa (point 2 in Fig. 7a), cracks 2^a and 2^b (Tensile crack) emanate at the upper and lower tips of crack, and then growth along the loading direction. At this moment, there is an obvious increase in AE event rate curve. When the specimen is loaded to 38.50 MPa (point 3 in Fig. 7(a)), crack 3 (Anti-tensile crack) initiates from the upper tip of crack, and then propagates along the direction of axial stress. Simultaneously, a distinct increase in AE event rate curve is observed. When the specimen is loaded to the peak strength of 45.01 MPa (point 4 in Fig. 7(a)), crack 4 (Anti-tensile crack) initiates from the lower tip of crack, and then propagates along the direction of axial stress, resulting in the stress drop of 3.54MPa. At the same time, an obvious increase appears in the AE event rate curve. When the specimen is loaded to 43.77 MPa (point 5 in Fig. 7(a)), cracks 5^a, 5^b, 5^c and 5^d (Far-field crack) emanate in specimen, which leads to that the AE event rate increases from low level to high level. Subsequently, the ultimate failure modes of specimen occur, as shown in Fig. 7(c). It is found from Fig. 7(b) that shear fracturing triggers the ultimate failure of red sandstone specimen containing pre-existing crack. According to the results shown in Fig. 6 and Fig. 7, the cracking process of specimen containing pre-existing crack is more progressive than that of intact specimen.

4. Time-frequency domain characteristics of AE signals for rocks

In this study, AE technology is used to monitor the fracture damage process of intact and cracked rocks subjected to uniaxial compression. The evolution characteristics of frequency of monitored AE signals are

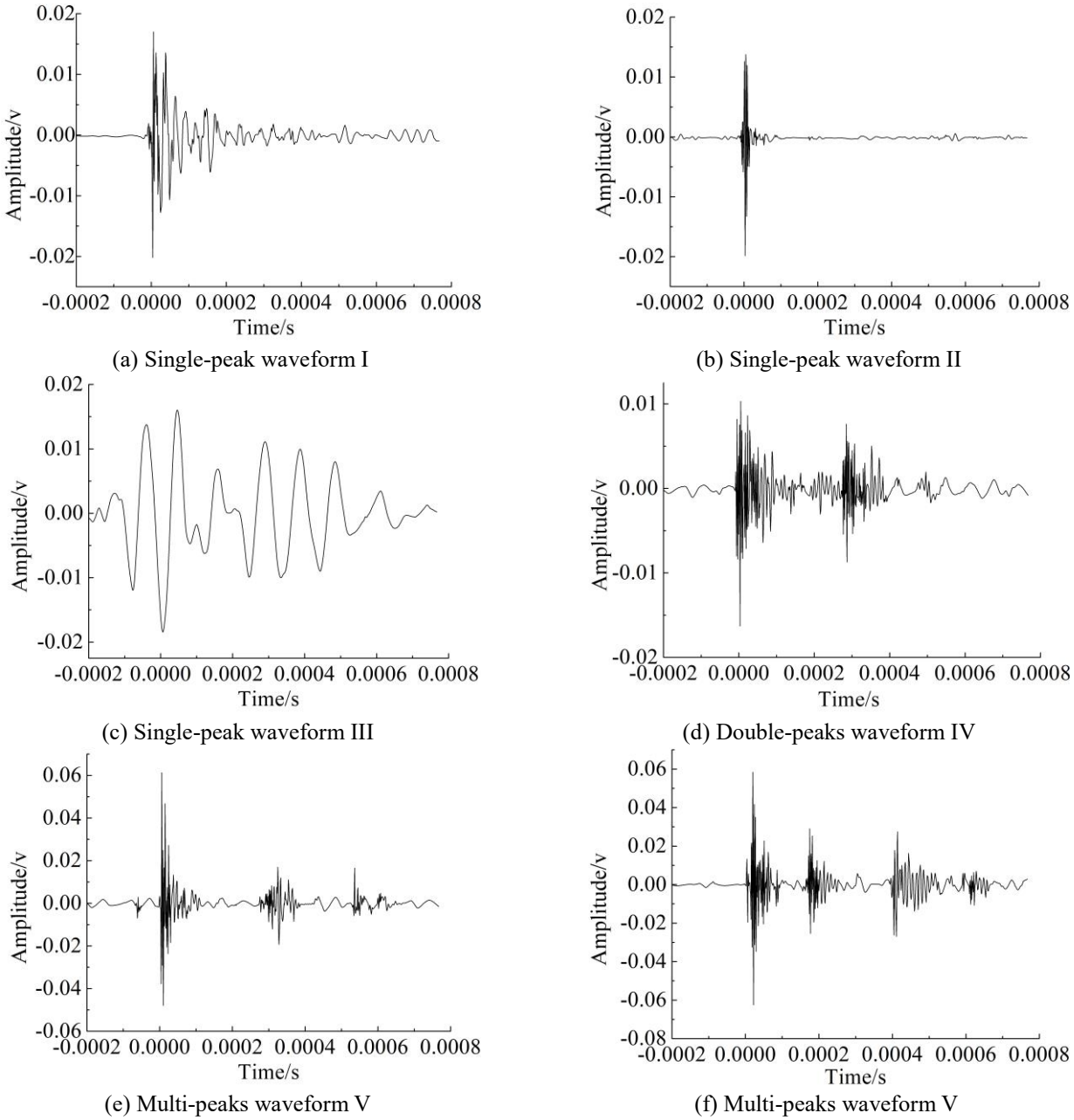

(a) Single-peak waveform I (b) Single-peak waveform II

(c) Single-peak waveform III (d) Double-peaks waveform IV

(e) Multi-peaks waveform V (f) Multi-peaks waveform V

Fig. 8 Different modes of AE waveform modes monitored during the cracking process of rocks

closely related to the nature of fracture events generated in the rocks (Cai and Zhao 2000, Zhao *et al.* 2006, Zhang *et al.* 2016). Consequently, in this study, the evolution characteristics of time-frequency domain for AE signals monitored at different loading stages of rocks are investigated using the STFT-based processing method.

4.1 Modes of AE signals monitored during the cracking process of rocks

A large number of AE signals are monitored during the entire cracking process of tested specimens. The total numbers of AE events for intact and cracked specimens are 3174 and 9938, respectively. However, the modes of AE waveforms are obviously different monitored during the loading process of specimens. To well distinguish the monitored AE signals, the time window length of AE waveforms is fixed, i.e., 8×10^{-4}s. In this paper, five different types of AE waveform modes are summarized, which are single-peak waveform I, single-peak waveform II, single peak waveform III, double-peaks waveform IV and multi-peaks waveform V, respectively. It is worth pointing out that the single-peak waveforms of I and II mostly occur in the stages of nonlinear compaction deformation and linear elastic for tested specimens. Two AE waveform modes, double-peaks waveform IV and multi-peaks waveform V, mainly appear after the stage of linear elastic. The single-peak waveform III mainly is observed when the catastrophic failure of tested specimens occurs. Fig. 8 shows the different modes of AE waveform monitored during the cracking process of rocks.

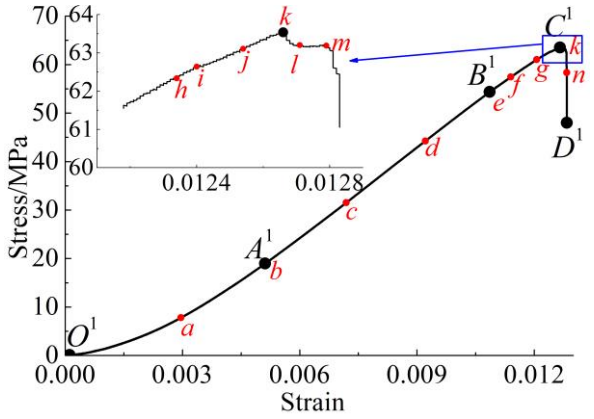

Fig. 9 AE signals selected during the deformation process of intact red sandstone specimen

Five modes of AE waveform are described as follows:

(1) Single-peak waveform I: AE signal consists of a basis waveform, which slowly attenuates as the time increases, as shown in Fig. 8(a). The fluctuation duration roughly lasts for 4×10^{-4}s when the amplitude of AE waveform attenuates 0 v. (2) Single-peak waveform II: AE signal consists of a single waveform, as shown in Fig. 8(b).

However, compared with the single-peak waveform I, the amplitude this AE signal quickly attenuates. Namely, the fluctuation time only about lasts for 0.5×10^{-4}s when the amplitude of AE waveform attenuates 0 v. (3) Single-peak waveform III: The duration of continuous fluctuation for this AE waveform lasts for 8×10^{-4}s when the amplitude attenuates to 0 v, as shown in Fig. 8(c). Note, the attenuation time of single-peak waveform III is obviously longer than that of I and II. (4) Double-peaks waveform IV: AE signal consists of two basic waveforms, as shown in Fig. 8(d). (5) Multi-peaks waveform V: AE signal consists of three or four basic waveforms, as shown in Figs. 8(e) and 8(f). The first basic AE waveform in this AE waveform has high amplitude. This AE signal usually accompanies the occurrence of macro-cracking. According to different modes of AE waveforms monitored during the cracking process of rocks, the time-frequency domain characteristics of AE signals are obtained by the SFFT method to further analyze the damage process of rocks.

4.2 Time-frequency domain characteristics of AE signals for intact rock

For intact specimen subjected to uniaxial compression, the deformation process is divided into four stages based on the curve of axial stress-strain. To intuitively visualize the time-frequency domain characteristics of AE waveforms, some typical AE signals are selected at different deformation stages of intact specimen. Fig. 9 shows the stress levels of selected AE signals in the stress-strain curve of intact specimen, which is denoted by some lower-case letters. Fig. 10 shows the selected AE waveforms processed by the wavelet as well as corresponding to the evolution characteristics of time-frequency domain obtained by the SFFT method. Figs. 10(a)-10(n) respectively correspond to lower-case letters marked in Fig. 9, i.e., *a*, *b*, *c*, *d*, *e*, *f*, *g*, *h*, *i*, *j*, *k*, *l*, *m* and *n*. In Fig. 10, the evolution characteristics of time-frequency domain for AE waveforms monitored at different deformation stages of rocks present obvious differences, which are analyzed in detail in this sub-section.

Fig. 10(a) shows the AE signal after de-noising and its time-frequency domain characteristics at point *a* in the nonlinear compaction stage. In Fig. 10(a), the mode of AE signal is single-peak waveform I. The frequency in the spectrum of AE signal is mainly distributed over the range of 20~400 kHz. The frequency distribution ranged from 100 to 400 kHz lasts for about 1×10^{-4}s. However, the low frequency distribution with the range of 20~100 kHz lasts for about 5×10^{-4}s, which is probably due to the existence of natural voids or cracks (Zhang *et al.* 2016). Moreover, monitored AE signals in this stage are all single-waveform I, which indicate that single micro-scale fracture event mainly occurs in the compaction stage.

Two modes of AE signals, including single-peak waveforms I and II, mainly appear in the elastic deformation stage of intact specimen, as shown in Figs. 10(b)-10(d). The modes of AE waveform change from single-peak waveform II (Figs. 10(b) and 10(c)) to single-peak waveform I (Fig. 10(d)) as the axial stress continuously increases. The distribution characteristics of frequency for both AE waveforms show obvious the similarities and the differences. Namely, the frequency distributions for these two types of AE waveforms are both over the range of 100~400 kHz. However, the frequency distribution for single-peak waveform II lasts for about 1×10^{-4}s. The frequency components for single-peak waveform I continues for about 4×10^{-4}s. Furthermore, compared with the nonlinear compaction stage, the frequency components ranged from 20 to 100 kHz is not observed in the linear stage. This characteristic can be used to identify the transformation from compaction to linear deformation. Similarly, single micro-scale fracture event mainly occurs in the linear elastic stage.

Figs. 10(e)-10(j) show the evolution characteristics of time-frequency domain of AE signals during the yield stage. It is seen from Figs. 10(e)-(j) that when the axial stress closes to peak strength, the modes of AE signals (Figs. 10(i)-(j)) are distinctly different from those of AE signals monitored early in this stage (Figs. 10(e) and 10(f)). That is to say, single-peak waveform I appears in the early stage of yield deformation. Compared with the compaction and elastic stages, the characteristics of frequency distribution for single-peak waveform I highlight some difference. Generally, the frequency components are primarily ranged from 10 to 500 kHz. The low frequency components with the range of 10~100 kHz lasts for about 6×10^{-4}s in the spectrum, which is different from that in the elastic stage. This probably due to that large number of micro-cracks nucleate and propagate during this stage, which is consistent with previous study (Zhang *et al.* 2016). Simultaneously, this result suggests that the deformation mechanism of rock changes at point *e*. When the axial stress closes to peak strength of intact specimen, AE signals with the modes of double-peaks waveform IV and multi-peaks waveform V begin to occur. At the same time, the instantaneous frequencies of AE signal in the spectrum are

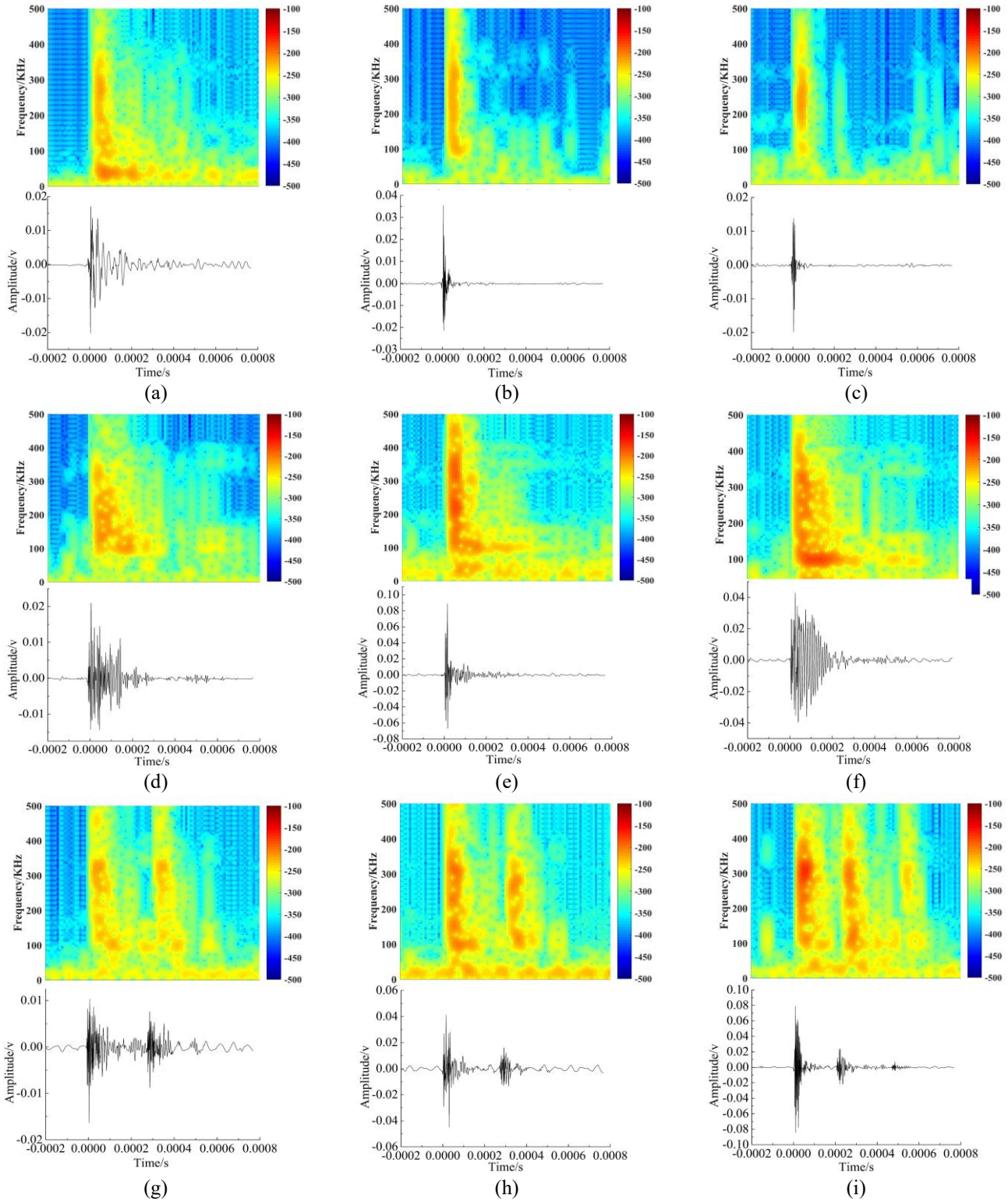

Fig. 10 AE signals after de-noising and time-frequency spectrums for intact specimen at different deformation stages

distributed over the range of 1~500 kHz. Among the low frequency components distributed from 1 to 50 kHz persists for the entire AE waveform, while the high frequency components (50~500 kHz) forms two or three band-shaped clusters, which indicate that macro-cracking events occur within rock due to the rapid propagation and coalescence of a large number of micro-cracks.

Fig. 10(k) shows the AE waveform and its spectrum at point k, i.e., the peak strength of specimen. AE signal with the mode of multi-peaks waveform V is monitored. The instantaneous frequencies are distributed from 1 to 500 kHz. The low frequency components with the range of 1~50 kHz persists for the entire AE waveform, and the frequency components distributed from 50 to 500 kHz forms four

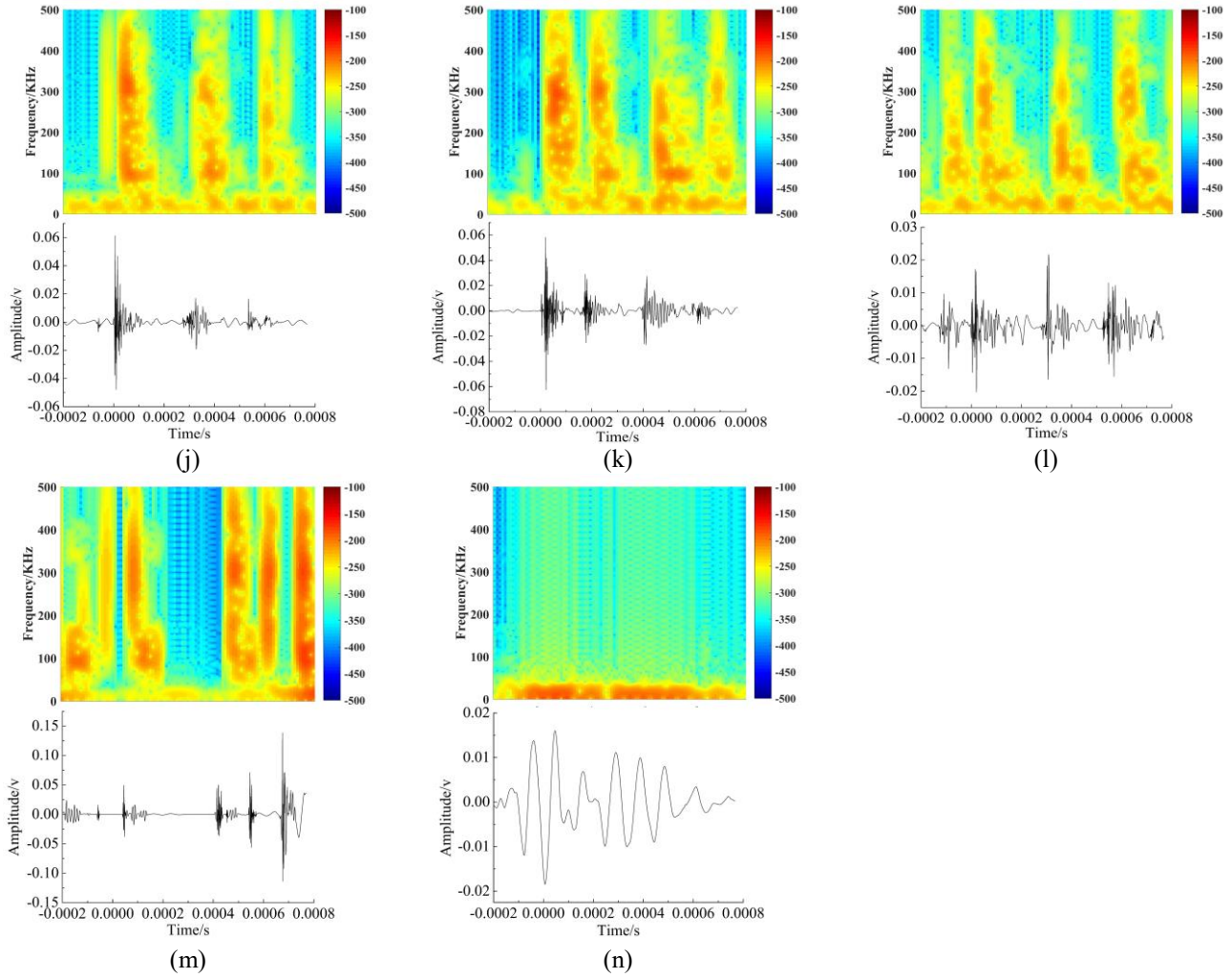

Fig. 10 Continued-

band-shaped clusters. Figs. 10(l) and 10(m) show the time-frequency domain characteristics during the failure stage. In Figs. 10(l) and 10(m), the distribution characteristics of frequency at points l and m are similar to those at point k. Note, five band-shaped clusters are observed in the spectrum of AE waveform when the specimen very closes to the ultimate failure. These results indicate that monitored AE signals become more complex than before in this stage, which is probably due to the initiation and propagation of macro-cracks. Fig. 10(n) shows the frequency characteristics of AE waveform monitored during the ultimate failure process in a very short time. Single-peak waveform III dominants this deformation process. Simultaneously, it can be found from Fig. 10(n) that the frequency characteristics of AE signal in this deformation process are completely different from those in other deformation processes. Namely, the low frequency components ranged from 1 to 50 kHz persists for the entire AE waveform.

4.3 Time-frequency domain characteristics of AE signals for intact rock

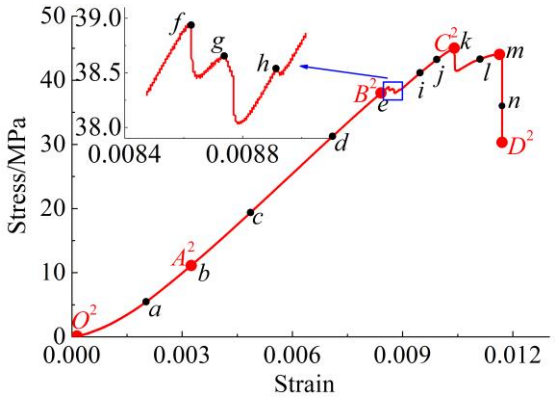

Fig. 11 AE signals selected during the deformation process of red sandstone specimen containing pre-existing crack

The deformation process of single crack-contained specimen is divided into four stages based on the evolution process of axial stress-strain curve. Likewise, some typical AE signals are selected at different deformation stages of cracked specimen to analyze the time-frequency domain characteristics of AE signals, as shown in Fig. 12. The selected AE signals correspond to some points in the stress-

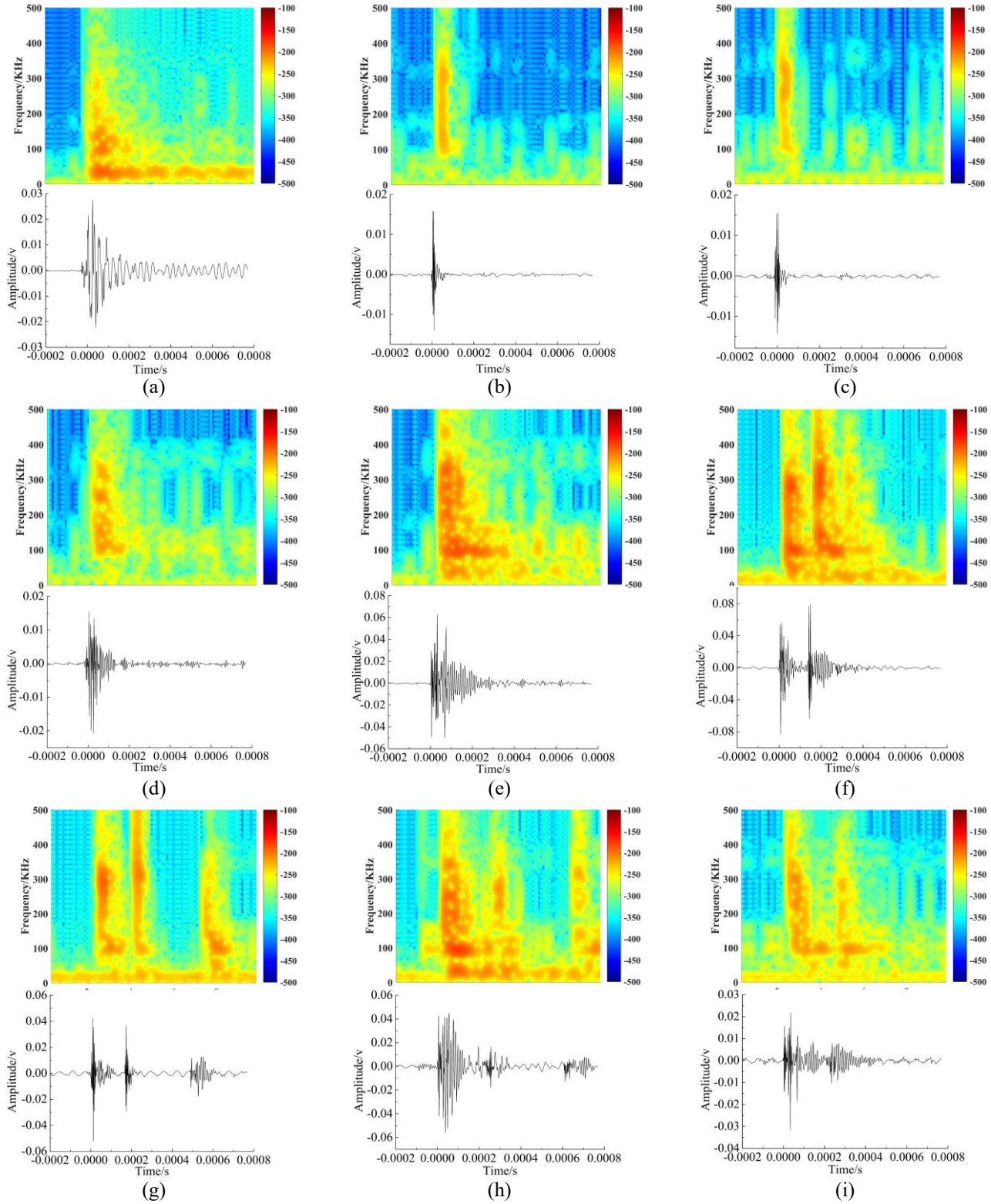

Fig. 12 AE signals after de-noising and time-frequency spectrums for specimen containing pre-existing crack at different deformation stages

strain curve, which are marked by some lower-case letters, as shown in Fig. 11. Figs. 12(a)-12(n) correspond to the points *a*, *b*, *c*, *d*, *e*, *f*, *g*, *h*, *i*, *j*, *k*, *l*, *m* and *n* shown in Fig. 11.

In Fig. 12, the time-frequency characteristics of AE signals highlight some differences at the different deformation stages of red sandstone specimen containing pre-existing crack, which are analyzed as follows:

It is seen from Figs. 10 and 12 that in the deformation stages of nonlinear compaction and elastic, the time-frequency domain characteristics of specimen containing

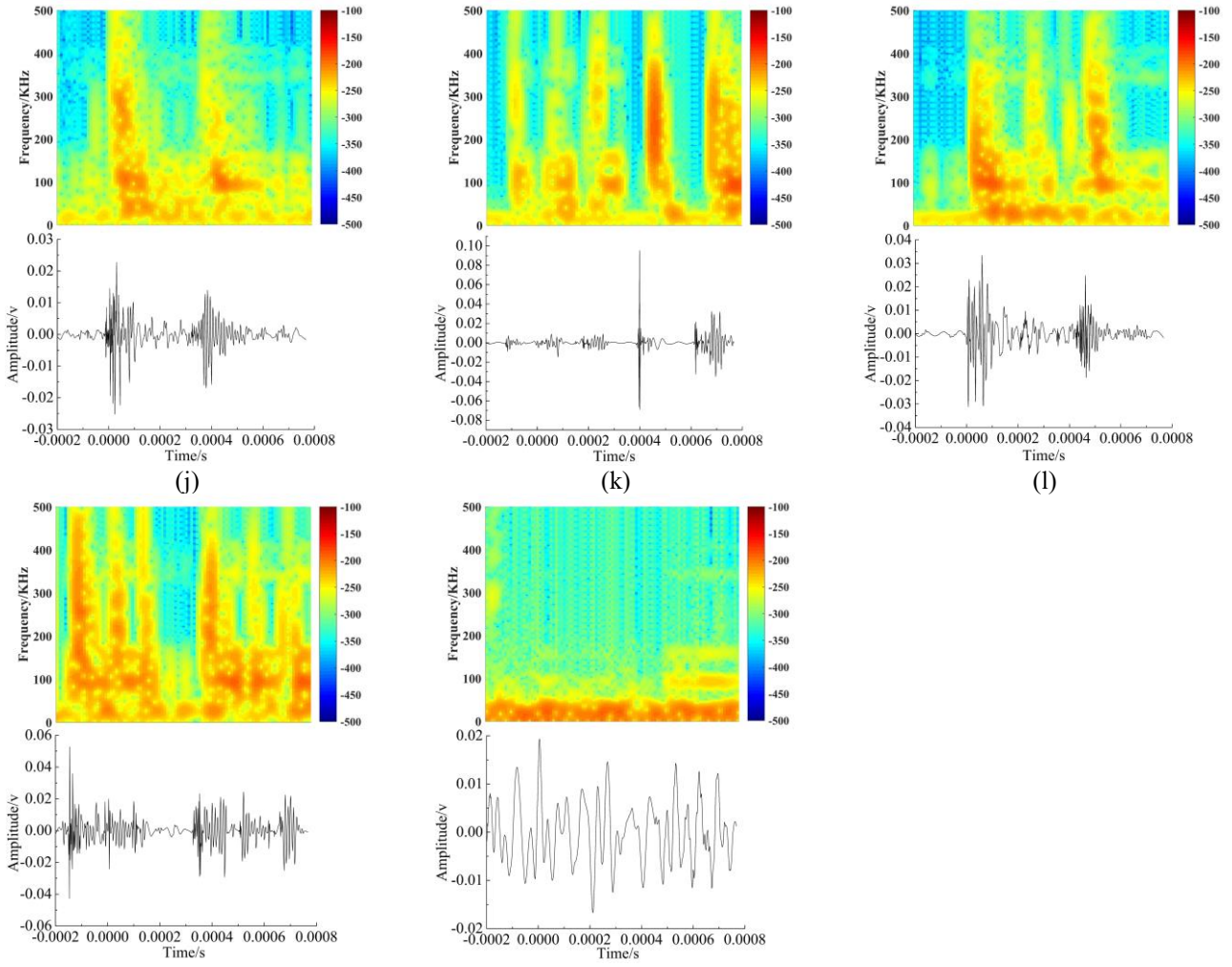

Fig. 12 Continued-

pre-existing crack are similar to those of intact specimen. Based on the analytical results in section 3, three macro-cracks initiate from the tips of crack during the stable macro-cracking stage of specimen containing pre-existing crack. Figs. 11(f)-11(h) depict the time-frequency domain characteristics of AE signals corresponding these three macro-cracking processes. In Figs. 11(f)-11(h), the evolution distribution of AE signals generated from each macro-cracking has similar characteristics. Generally, AE signal with the mode of multi-peaks waveform V is monitored for each macro-cracking. The low frequency components with the range of 1~50 kHz lasts for about 8×10^{-4}s, and the frequency components distributed from 50 to 500 kHz form three band-shaped clusters. Figs. 11(i) and 11(j) show the AE signals after macro-cracking. In Figs. 11(i) and 11(j), AE signals with the mode of double-peaks waveform IV are monitored at points *i* and *j* in the stress-strain curve of specimen containing pre-existing crack, and the frequency components ranged from 100 to 500 kHz form two band-shaped clusters in the spectra.

Figs. 11(k)-11(n) show the time-frequency domain characteristics of AE signal in the stage of unstable macro-cracking and failure for specimen containing pre-existing crack. In Figs. 11(k)-11(m), the mode of AE signals is multi-peaks waveform V. At the same time, the instantaneous frequency of AE signals is distributed from 1 to 500 kHz. The low frequency components with the range of 1~50 kHz maintains for the entire AE waveform. Moreover, the frequency components varied from 50~500 kHz forms five band-shaped clusters when macro-cracks initiate and propagate unstably, as shown in Figs. 11(k) and 11(m). These results indicate that the occurrence of unstable macro-cracking leads to the generation of complex AE signals. Fig. 11(n) shows the frequency distribution of AE signal monitored during the ultimate failure of specimen containing pre-existing crack in a very short time. In Fig. 11(n), single-peak waveform III is monitored, and the low frequency components ranged from 1 to 50 kHz persists for the entire AE waveform, which are similar to those of intact specimen.

5. Discussions

The AE signals monitored during the deformation failure process of rocks are closely related to the its fracture

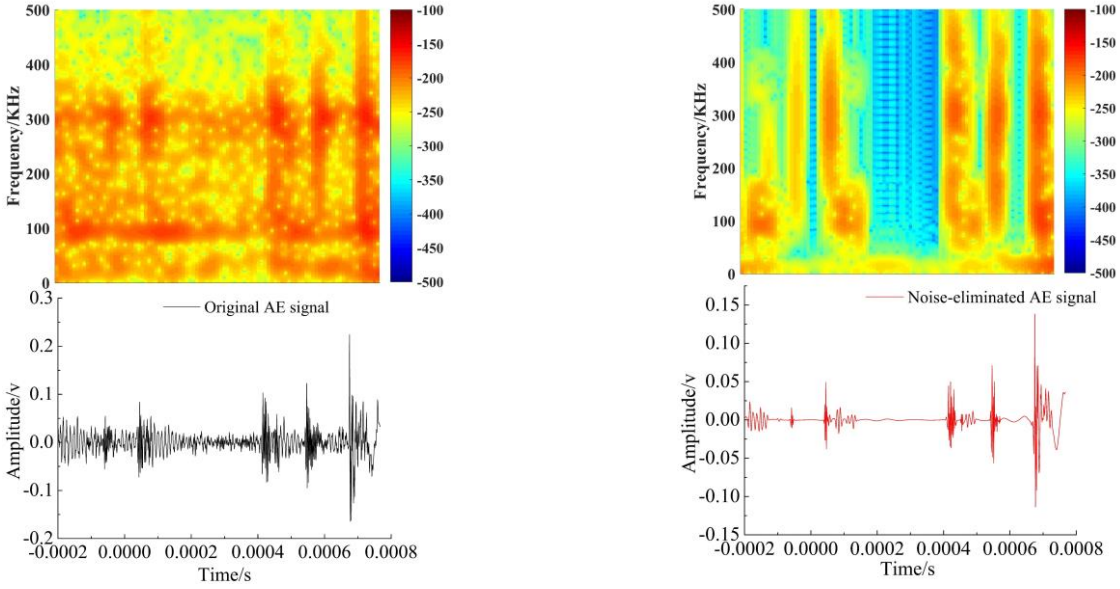

(a) original AE waveform (b) AE waveform after de-noising

Fig. 13 AE waveforms and its time-frequency domain spectra

damage (Liu *et al*. 2021, Du *et al*. 2022, Niu *et al*. 2023b).

The evolution characteristics of frequency component of AE signals (Benson *et al.* 2010, Zhang *et al.* 2016, Patricia and Celestino 2019, Du *et al*. 2020, Li *et al*. 2021, Dinmohammadpour *et al.* 2022) are sensitive to the deformation failure process of rocks. To well present the spectral components of AE waveforms in different instantaneous times, the short-time Fourier transform (STFT) method is employed to gain the evolution characteristics of time-frequency domain presented as spectrograms. However, some unavoidable external factors result in that monitored AE waveforms carry some noises components unrelated to rock fracture (Benson *et al.* 2010, Zhang *et al.* 2016, Patricia and Celestino 2019, Du *et al*. 2020). The noises mainly come from the friction and dislocation of contact surfaces between the testing machine and specimen as well as between the AE probe and specimen. The existence of noises heavily disturbs the distribution characteristics of time-frequency domain of AE waveforms. Therefore, the noises carrying in AE waveforms are eliminated by the method of wavelet (Deng *et al.* 2020) before the STFT processing. Figs. 13(a) and 13(b) show the time-frequency domain characteristics of original AE signal and AE signal after de-noising, respectively. In Figs. 13(a) and 13(b), AE waveform after de-noising is more concise that original AE waveform. In addition, the frequency components related to the noises are obviously eliminated. These results suggest that the AE waveform after de-noising can well reflect the essence of rock fracture.

Based on the analytical results in section 4, the modes of AE signals are distinctly different at different deformation stages of rocks as well as the time-frequency domain characteristics of AE signals, which can be employed to characterize the damage evolution and to reveal the deformation mechanism of rocks. For intact and cracked rocks, the modes and the time-frequency domain distribution characteristics for monitored AE signals present the same evolution results in the stages of nonlinear compaction and linear elastic. Namely, two modes of AE signals including single-peak waveforms I and II are mainly monitored, indicating that single fracture event occurs in these two stages. The frequency components are mainly distributed from 20 to 400 kHz in the nonlinear compaction stage. While the frequency components are mostly ranged from 100 to 500 kHz in the elastic stage. The disappearance of frequency components with the 20~100 kHz range can failure.

Based on the analytical results in section 3, the cracking process of specimen containing pre-existing crack is more progressive than that of intact specimen, leading to that the types and the time-frequency domain characteristics of AE waveforms present obvious differences. In general. when cracked specimen enters into the stage of stable macro-cracking, each macro-cracking generates a number of AE signals with the mode of multi-peaks waveform V. Simultaneously, the distribution characteristics of frequency present three band-shaped clusters in the spectra of AE signals. Compared with the stable macro-cracking stage, AE signals of multi-peaks waveform V are also monitored in the stage of unstable macro-cracking and failure. Whilst the frequency distributions with four or five band-shaped clusters in the spectra dominate this deformation process.

The evolution characteristics for the modes and frequency of AE signals indicate that the deformation mechanism of specimen containing pre-existing crack is unstable and the ultimate failure is about to occur. To summarize, the frequency distribution with multiple band-shaped clusters can be regarded as the early warning for the instability of rock containing pre-existing crack.

Moreover, the difference of deformation mechanism of rocks in the deformation process results in the occurrence of

low frequency components with different distribution characteristics in the spectra of AE signals. In the nonlinear deformation stage, the low frequency components with the range of 20~100 kHz occur, which are caused by the existence of micro-voids and micro-cracks (Zhang *et al.* 2016). However, the low frequency components with the range of 10~100 kHz occur in the spectra of AE signals monitored after the elastic deformation of intact and cracked specimens as well as maintain for the entire AE waveforms. This phenomenon indicates a change in the deformation mechanism of rocks (Zhang *et al.* 2016). Namely, a number of micro-cracks nucleate, initiate, propagate and coalesce after the elastic deformation. Subsequently, when some macro-cracks initiate and propagate, the low frequency components ranged from 1 to 50 kHz are observed in in the spectra of AE signals. These cracking processes aggravate the damage degree within rock, which can be reflected by the attenuation of frequency. In other words, the attenuation of frequency enables the exploration of rock failure trends, which is consistent with the results in the previous study (Zhang *et al.* 2016).

6. Conclusions

Uniaxial compression testes are performed on the intact and cracked red sandstone specimens. The cracking process of rocks are monitored by AE and photographic techniques. This study presents a STFT-based AE processing approach to analyze the deformation damage characteristics of rocks.

The following main conclusions are drawn:

• The cracking process of specimen containing pre-existing crack is more progressive than that of intact specimen. The inter-event time function $F(\tau)$ can reliably characterize the fracture damage characteristics of intact and cracked rocks under uniaxial compression.

• Five modes of AE waveform are observed during the deformation process of intact and cracked specimens, including single-peak waveform I, single-peak waveform II, single-peak waveform III, double-peaks waveform IV and multi-peaks waveform V. The modes of AE signals are different at different deformation stages of rocks.

• The evolution characteristics of time-frequency domain of AE signals present obvious differences during the loading process of rocks. The distribution characteristics of frequency changing from a single band-shaped cluster to multiple band-shaped clusters imply that the deformation mechanism of rock is unstable. This phenomenon can be regarded as an early warning information of failure for rocks.

• The low frequency components with different distribution characteristics in the spectra indicate that different deformation mechanism of rocks. The compaction of micro-voids and micro-cracks generates the low frequency components ranged from 20 to 100 kHz. The damage accumulation caused by initiation and propagation of new micro-cracks and macro-cracks produces the low frequency components distributed from 10 to 100 kHz and 1 to 50 kHz. The attenuation of frequency enables the exploration of rock failure trends.

Acknowledgments

The research described in this paper was financially supported by the Shaoxing Basic Public Welfare Planning Project (Grant Nos. 2022A13004), the National Natural Science Foundation of China (Grant No. 41977256), the Zhejiang Natural Science Foundation (Grant No. LHZ21D020001) and the Scientific Research Fund Project of Shaoxing University (Grant No. 2021LG014).

References

Benson, P.M., Vinciguerra, S., Meredith, P.G. and Young, R.P. (2010), "Spatio-temporal evolution of volcano seismicity: a laboratory study", *Earth Planet. Sci. Lett*., **297**(1-2), 315-323. https://doi.org/10.1016/j.epsl.2010.06.033.

Berto, F. and Lazzarin, P. (2014), "Recent developments in brittle and quasi-brittle failure assessment of engineering materials by means of local approaches", *Mat. Sci. Eng. R.*, **75**, 1-48. https://doi.org/10.1016/j.mser.2013.11.001.

Berto, F., Lazzarin, P. and Ayatollahi, M.R. (2013), "Brittle failure of inclined key-hole notches in isostatic graphite under in-plane mixed mode loading", *Fatigue Fract. Eng. Mater. Struct*., **36**(9), 942-955. https://doi.org/10.1111/ffe.12057.

Cai, J.G. and Zhao, J. (2000), "Effects of multiple parallel fractures on apparent attenuation of stress waves in rock masses", *Int. J. Rock Mech. Min. Sci*., **37**(4), 661-682. https://doi.org/10.1016/S1365-1609(00)00013-7.

Deng, Z.H., Wang, J.W., Liang, X.Y. and Liu, N. (2020), "Function extension based real-time wavelet de-noising method for projectile attitude measurement", *Sensors*., **20**(1), 200. https://doi.org/10.3390/s20010200.

Du, K., Li, X.F., Tao, M. and Wang, S.F. (2020), "Experimental study on acoustic emission (AE) characteristics and crack classification during rock fracture in several basic lab tests", *Int. J. Rock Mech. Min. Sci.*, **133**, 104411. https://doi.org/10.1016/j.ijrmms.2020.104411.

Dinmohammadpour, M., Nikkhah, M., Goshtasbi, K. and Ahangari, K. (2022), "Application of wavelet transform in evaluating the Kaiser effect of rocks in acoustic emission test", *Measurement.*, **192**, 110887. https://doi.org/10.1016/j.measurement.2022.110887.

Du, K., Sun, Y., Zhou, J., Khandelwal, M. and Gong, F.Q. (2022), "Mineral Composition and Grain Size Effects on the Fracture and Acoustic Emission (AE) Characteristics of Rocks Under Compressive and Tensile Stress", *Rock Mech. Rock Eng.*, **55**(10),6445-6474. https://doi.org/10.1007/s00603-022-02980-y.

Huang, J., Qin, C.Z., Niu, Y., Li, R., Song, Z.L. and Wang, X.D. (2022), "A method for monitoring acoustic emissions in geological media under coupled 3-D stress and fluid flow", *J. Petrol. Sci. Eng*., **211**, 110227. https://doi.org/10.1016/j.petrol.2022.110227.

He, M.C., Miao, J.L. and Feng, J.L. (2010), "Rock burst process of limestone and its acoustic emission characteristics under true-triaxial unloading conditions", *Int. J. Rock Mech. Min. Sci.*, **47**(2), 286-298. https://doi.org/10.1016/j.ijrmms.2009.09.003.

Kong, F.M., Xue, Y.G., Qiu, D.H., Li, Z.Q., Chen, Q.Q. and Song, Q. (2021), "Impact of grain size or anisotropy on correlations between rock tensile strength and some rock index properties",

Geomech. Eng., **27**(2), 131-150. https://doi.org/10.12989/gae.2021.27.2.131.

Kim, J.W., Chong, S.H. and Cho, G.C. (2022), "Probabilistic Q-system for rock classification considering shear wave propagation in jointed rock mass", *Geomech. Eng.*, **30**(5), 449-460. https://doi.org/10.12989/gae.2022.30.5.449.

Liu, L.W., Li, H.B., Li, X.F., Wu, D. and Zhang, G.K. (2021), "Underlying mechanisms of crack initiation for granitic rocks containing a single pre-existing flaw: Insights from Digital Image Correlation (DIC) Analysis", *Rock Mech. Rock Eng.*, **54**(2): 857-873. https://doi.org/10.1007/s00603-020-02286-x.

Li, X.L., Chen, S.J., Liu, S.M. and Li, Z.H. (2021), "AE waveform characteristics of rock mass under uniaxial loading based on Hilbert-Huang transform", *J. Cent. South Univ.*, **28**, 1843-1856. https://doi.org/10.1007/s11771-021-4734-6.

Liu, X.L., Liu, Z., Li, X.B., Gong, F.Q. and Du, K. (2020), "Experimental study on the effect of strain rate on rock acoustic emission characteristics", *Int. J. Rock Mech. Min. Sci.*, **133**, 104420. https://doi.org/10.1016/j.ijrmms.2020.104420.

Liu, J.P., Li, Y.H., Xu, S.D., Xu, S., Jin, C.Y. and Liu, Z.S. (2015), "Moment tensor analysis of acoustic emission for cracking mechanisms in rock with a pre-cut circular hole under uniaxial compression", *Eng. Fract. Mech.*, **135**, 206-218. https://doi.org/10.1016/j.engfracmech.2015.01.006.

Lin, P., Wong, R.H.C. and Tang, C.A. (2015), "Experimental study of coalescence mechanisms and failure under uniaxial compression of granite containing multiple hoes", *Int. J. Rock Mech. Min. Sci.*, **77**, 313-237. https://doi.org/10.1016/j.ijrmms.2015.04.017.

Lu, C.P., Dou, L.M., Liu, H., Liu, H.S., Liu, B. and Du, B.B. (2012), "Case study on microseismic effect of coal and gas outburst process", *Int. J. Rock Mech. Min. Sci.*, **53**, 101-110. https://doi.org/10.1016/j.ijrmms.2012.05.009.

Li, L.R., Deng, J.H., Zheng, L. and Liu, J.F. (2017), "Dominant frequency characteristics of acoustic emissions in white marble during direct tensile tests", *Rock Mech. Rock Eng.*, **50**(5), 1337-1346. https://doi.org/10.1007/s00603-016-1162-2.

Miao, S.T., Pan, P.Z., Zhao, X.G., Shao, C.Y. and Yu, P.Y. (2021), "Experimental Study on Damage and Fracture Characteristics of Beishan Granite Subjected to High-temperature Treatment with DIC and AE Techniques", *Rock Mech. Rock Eng.*, **54**(2), 721-743. https://doi.org/10.1007/s00603-020-02271-4.

Moradian, Z., Einstein, H.H. and Ballivy, G. (2016), "Detection of cracking levels in brittle rocks by parametric analysis of the acoustic emission signals", *Rock Mech. Rock Eng.*, **49**(3), 785-800. https://doi.org/10.1007/s00603-015-0775-1.

Niu, Y. and Zhou, X.P. (2021), "Forecast of time-of-instability in rocks under complex stress conditions using spatial precursory AE response rate", *Int. J. Rock Mech. Min. Sci.*, **147**, 104908. https://doi.org/10.1016/j.ijrmms.2021.104908.

Niu, Y., Wang J.G., Wang, X.K., Hu, Y.J., Zhang J.Z., Zhang R.R. and Hu Z.J. (2023a) "Numerical study on cracking behaviors and fracture failure mechanism of flawed rock materials under uniaxial compression", *Fatigue Fract. Eng. Mater. Struct.*, 1-16. https://doi.org/10.1111/FFE.13983.

Niu, Y., Hu, Y.J. and Wang, J.G. (2023b), "Cracking characteristics and damage assessment of filled rocks using acoustic emission technology", *Int. J. Geomech.*, **23**(4), 04023013. https://doi.org/10.1061/IJGNAI.GMENG-8034.

Patricia, R. and Celestino, T.B. (2019), "Application of acoustic emission monitoring and signal analysis to the qualitative and quantitative characterization of the fracturing process in rocks", *Eng. Fract. Mech.*, **210**, 54-69. https://doi.org/10.1016/j.engfracmech.2018.06.027.

Pakzad, R., Wang, S.Y. and Sloan, S. (2018), "Numerical study of the failure response and fracture propagation for rock specimens with preexisting flaws under compression", *Int. J. Geomech.*, **18**(7), 04018070. https://doi.org/10.1061/(ASCE)GM.1943-5622.0001172.

Shukla, R., Ranijith, P.G., Choi, S.K., Haque, A., Yellishetty, M. and Hong, L. (2013), "Mechanical behavior of reservoir rock under brine saturation", *Rock Mech. Rock Eng.*, **46**(1), 83-93. https://doi.org/10.1007/s00603-012-0246-x.

Shi, H., Zhang, H.Q. and Song, L. (2020), "Evolution of sandstone shear strength parameters and its mesoscopic", *Geomech. Eng.*, **20**(1), 29-41. https://doi.org/10.12989/gae.2020.20.1.029.

Sun, W., Du, H., Zhou, F. and Shao, J. (2019), "Experimental study of crack propagation of rock-like specimens containing conjugate fractures", *Geomech. Eng.*, **17**(4), 323-331. https://doi.org/10.12989/gae.2019.17.4.323.

Triantis, D. and Kourkoulis, S.K. (2018), "An alternative approach for representing the data provided by the acoustic emission technique", *Rock Mech. Rock Eng.*, **51**(8), 2433-2438. https://doi.org/10.1007/s00603-018-1494-1.

Wasantha, P.L.P., Ranjith, P.G. and Shao, S.S. (2014), "Energy monitoring and analysis during deformation of bedded-sandstone: use of acoustic emission", *Ultrasonics.*, **54**(1), 217-226. https://doi.org/10.1016/j.ultras.2013.06.015.

Wang, Y.T., Zhou, X.P. and Shou, Y.D. (2017), "The modeling of crack propagation and coalescence in rocks under uniaxial compression using the novel conjugated bond-based peridynamics", *Int. J. Mech. Sci.*, **128**, 614-643. https://doi.org/10.1016/j.ijmecsci.2017.05.019.

Wong, L.N.Y. and Xiong, Q.Q. (2018), "A method for multiscale interpretation of fracture processes in carrara marble specimen containing a single flaw under uniaxial compression", *J. Geophys. Res-Sol. Ea.*, **123**(8), 3459-6490. https://doi.org/10.1029/2018JB015447.

Wang, Y.T., Zhou, X.P., Wang, Y. and Shou, Y.D. (2018), "A 3-D conjugated bond-pair-based peridynamic formulation for initiation and propagation of cracks in brittle solids", *Int. J. Solids Struct.*, **134**, 89-115. https://doi.org/10.1016/j.ijsolstr.2017.10.022.

Wang, Y.S., Deng, J.H., Li, L.R. and Zhang, Z.H. (2019), "Micro-failure analysis of direct and flat loading Brazilian tensile tests", *Rock Mech. Rock Eng.*, **52**(11), 4175-4187. https://doi.org/10.1007/s00603-019-01877-7.

Wong, L.N.Y. and Einstein, H.H. (2009), "Systematic evaluation of cracking behavior in specimens containing single flaws under uniaxial compression", *Int. J. Rock Mech. Min. Sci.*, **46**(2), 239-249. https://doi.org/10.1016/j.ijrmms.2008.03.006.

Yang, S.Q., Jing, H.W., Huang, Y.H., Ranjith, P.G. and Jiao, Y.Y. (2014), "Fracture mechanical behavior of red sandstone containing a single fissure and two parallel fissures after exposure to different high temperature treatments", *J. Struct. Geol.*, **69**, 245-264. https://doi.org/10.1016/j.jsg.2014.10.014.

Zheng, Q.Q., Xu, Y., Hu, H., Qian, J.W., Ma, Y. and Gao, X. (2021), "Quantitative damage, fracture mechanism and velocity structure tomography of sandstone under uniaxial load based on acoustic emission monitoring technology", *Constr. Build. Mater.*, **272**, 121911. https://doi.org/10.1016/j.conbuildmat.2020.121911.

Zhao, J.S., Jiang, Q., Lu, J.F., Chen, B.R., Pei, S.F. and Wang, Z.L. (2022), "Rock fracturing observation based on microseismic monitoring and borehole imaging: In situ investigation in a large underground cavern under high geo-stress", *Tunn. Undergr. Sp. Tech.*, **126**, 104549. https://doi.org/10.1016/j.tust.2022.104549.

Zhou, X.P. and Zhang, J.Z. (2021), "Damage progression and acoustic emission in brittle failure of granite and sandstone", *Int. J. Rock Mech. Min. Sci.*, **143**, 104789. https://doi.org/10.1016/j.ijrmms.2021.104789.

Zhang, J.Z., Zhou, X.P., Zhu, J.Y., Xian, C. and Wang, Y.T. (2018), "Quasi-static fracturing in double-flawed specimens under uniaxial loading: The role of strain rate", *Int. J. Fract.*, **211**(1-2),

75-102. https://doi.org/10.1007/s10704-018-0277-8.

Zhou, X.P., Niu, Y., Zhang, J.Z., Shen, X.C., Zheng, Y. and Berto, F. (2019), "Experimental study on effects of freeze-thaw fatigue damage on the cracking behaviors of sandstone containing two unparallel fissures", *Fatigue Fract. Eng. Mater. Struct.*, **42**(6), 1322-1340. https://doi.org/10.1111/ffe.12987.

Zhou, X.P., Lian, Y.J., Wong, L.N.Y. and Berto, F. (2018), "Understanding the fracture behavior of brittle and ductile multi-flawed rocks by uniaxial loading by digital image correlation", *Eng. Fract. Mech.*, **199**, 438-460. https://doi.org/10.1016/j.engfracmech.2018.06.007.

Zhang, R., Dai, F., Gao, M.Z., Xu, N.W. and Zhang, C.P. (2015), "Fractal analysis of acoustic emission during uniaxial and triaxial loading of rock", *Int. J. Rock Mech. Min. Sci.*, **79**, 241-249. https://doi.org/10.1016/j.ijrmms.2015.08.020.

Zheng, Z.H., Deng, J.H., Zhu, J.B. and Li, L.R. (2018), "An experimental investigation of the failure mechanisms of jointed and intact marble under compression based on quantitative analysis of acoustic emission waveforms", *Rock Mech. Rock Eng*., **51**(7), 2299-2307. https://doi.org/10.1007/s00603-018-1484-3.

Zhang, J., Peng, W.H., Liu, F.Y., Zhang, H.X. and Li, Z.J. (2016), "Monitoring rock failure processes using the hilbert–huang transform of acoustic emission signals", *Rock Mech. Rock Eng.*, **49**(2), 427-442. https://doi.org/10.1007/s00603-015-0755-5.

Zhao, J., Zhao, X.B. and Cai, J.G. (2006), "A further study of P-wave attenuation across parallel fractures with linear deformational behaviour", *Int. J. Rock Mech. Min. Sci.*, **43**(5), 776-788. https://doi.org/10.1016/j.ijrmms.2005.12.007.

Zhao, W., Huang, R. and Yan, M. (2015), "Mechanical and fracture behavior of rock mass with parallel concentrated joints with different dip angle and number based on PFC simulation", *Geomech. Eng.*, **8**(6), 757-767. https://doi.org/10.12989/gae.2015.8.6.757.

Zhu, X. and Liu, W. (2018), "The rock fragmentation mechanism and plastic energy dissipation analysis of rock indentation", *Geomech. Eng.*, **16**(2), 195-204. https://doi.org/10.12989/gae.2018.16.2.195.

CC